Appl. Phys. A (2014) 116:333–340
DOI 10.1007/s00339-013-8126-0

Applied Physics A
Materials Science & Processing

The electronic structure, electronic charge density and optical properties of the diamond-like semiconductor Ag_2ZnSiS_4

A. H. Reshak · Sikander Azam

Received: 16 February 2013 / Accepted: 29 October 2013 / Published online: 19 November 2013

Abstract The electronic structure, electronic charge density and optical properties of the diamond-like semiconductor Ag_2ZnSiS_4 compound with the monoclinic structure have been investigated using a full-relativistic version of the full-potential augmented plane-wave method based on the density functional theory, within local density approximation (LDA), generalized gradient approximation (GGA), Engel–Vosko GGA (EVGGA) and modified Becke Johnson (mBJ) potential. Band structures divulge that this compound is a direct energy band gap semiconductor. The obtained energy band gap value using mBJ is larger than those obtained within LDA, GGA and EVGGA. There is a strong hybridization between Si-s and S-s/p, Si-p and Zn-s, Ag-s/p and Zn-s, and Ag-s and Ag-p states. The analysis of the site and momentum-projected densities shows that the bonding possesses covalent nature. The dielectric optical properties were also calculated and discussed in detail.

1 Introduction

Over the last few years, multi-cation diamond-like semiconductors (DLSs) have got a swelled courtesy for their auspicious physical properties. A work by Shi et al. [1] displayed that $Cu2Sn_{1-x}$ In_xSe_3 possess an effective thermoelectric figure of worth, ZT, of 1.14 at 850 K, demonstrating its potential usage in thermoelectric functions. A contemporary exertion on the compound $Cu_2ZnSnSe_4$ (CZTSe) has revealed that the substitution of In by Sn increases ZT from 0.28 in the intuitive compound to 0.95 in the 10 % In substituted phase [2]. Additional work by Steinhagen et al. [3] has verified that Cu_2ZnSnS_4 (CZTS) can be blended as nanocrystals in the kesterite structure which can be used as an inexpensive means for the fabrication of photovoltaic devices. Moreover, in 2009, Lekse et al. [4] reported that Li_2CdSnS_4 demonstrates a second harmonic generation (SHG) that is 100× that of α-quartz and is phase matchable. They imply that quaternary DLSs with better band gaps should hold increased laser damage thresholds in contrast to the lucratively available ternary DLSs that are presently used in nonlinear optical devices [5, 6]. Recently, Brunetta et al. [10] have synthesized Ag_2ZnSiS_4 single crystal. They have calculated the electronic band structure and density of states of Ag_2ZnSiS_4 compound using the full-potential linearized augmented plane-wave (FPLAPW) method as implemented in WIEN2k program within GGA approximation. The obtained band gap (1.8 eV) was understated by around 1.3 eV than the measured one (2.51 eV).

All the above-mentioned compounds have the diamond-like structure, i.e., they have a structure that look likes either cubic or hexagonal diamond [7, 8]. These resources follow a set of guiding principle that consist of: (1) each atom ought to have a common valence electron concentration of four; (2) the average concentration of valence electrons for each anion is required to be eight [7, 8]; (3) each atom be obliged to have a tetrahedral coordination; and (4) the octet of each anion should be contented by its nearest neighbors [7–9]. These guiding principles can be used not only to organize the known compounds, but also to envisage new compounds.

A. H. Reshak · S. Azam (✉)
New Technologies - Research Center, University of West Bohemia, Univerzitni 8, Pilsen 306 14, Czech Republic
e-mail: sikander.physicst@gmail.com

A. H. Reshak
Center of Excellence Geopolymer and Green Technology, School of Material Engineering, University Malaysia Perlis, 01007 Kangar, Perlis, Malaysia

In the current paper, we demonstrate the results of the diamond-like semiconductor Ag_2ZnSiS_4 compound. The electronic band structure, density of states, charge density and optical properties of this compound were calculated and analyzed.

2 Methodology

The crystal structure of Ag_2ZnSiS_4 compounds is shown in Fig. 1. The compound has monoclinic structure with space group # 7 (Pn). The lattice constants for the Ag_2ZnSiS_4 compound are $a = 6.4052(1)$ Å, $b = 6.5484(1)$ Å, $c = 7.9340(1)$ Å, $\beta = 90.455(1)^{\circ}$ [10]. The optimized atomic positions in comparison with the experimental one [10] are shown in Table 1. The electronic structure and optical properties of Ag_2ZnSiS_4 compound are studied by using the full-potential linearized augmented plane wave as implemented in the WIEN2k code [11]. The perspective is supported by density functional theory (DFT) [12, 13]. The exchange correlation potential E_{xc} was evaluated by means of local density approximation (LDA), generalized gradient approximation (GGA), EVGGA as modulated by Engel and Vosko [14–17] and modified Becke and Johnson (mBJ). Kohn–Sham wave functions were protracted in sustenance of spherical harmonic function inside the non-overlapping muffin-tin (MT) spheres and among Fourier series in the interstitial region. The *l*-expansions of the wave functions were forfeited out up to $l_{max} = 10$ within the muffin-tin spheres of radius R_{MT}, while the charge density the Fourier was expanded up to $G_{max} = 12$. In the interstitial regions the wave functions were distended in the plane waves for the cut off of $K_{max} \times R_{MT} = 7.0$ in order to achieve the convergence for energy eigenvalues. The valves for muffin-tin radii R_{MT} was chosen for Ag_2ZnSiS_4 compound: R_{MT} (Ag) = 2.38, R_{MT} (Si) = 1.89, R_{MT} (Zn) = 2.20 and R_{MT} (S) = 1.89 a.u.

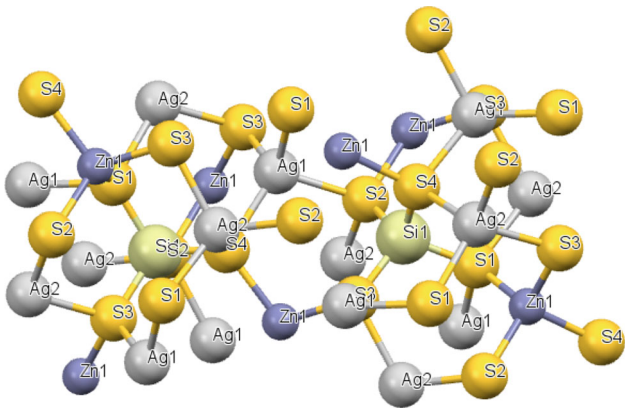

Fig. 1 Unit cell structure

For the optical properties, the dielectric function was premeditated in the momentum representation, which requires matrix elements of the momentum p among occupied and unoccupied states. As a result, the components of the imaginary part of the dielectric function, $\varepsilon_2^{ij}(\omega)$ was computed by using [18] the relation

$$\varepsilon_2^{ij}(\omega) = \frac{4\pi^2 e^2}{Vm^2\omega^2} \times \sum_{knn'\sigma} \langle kn\sigma|p_i|kn'\sigma\rangle\langle kn'\sigma|p_j|kn\sigma\rangle \times f_{kn}(1 - f_{kn'})\sigma(E_{kn'} - E_{kn} - \hbar\omega)$$

where e, m, ω and V are the electron charge, mass, frequency of the incoming electromagnetic radiation and the volume of the unit cell, respectively, where $(p_x, p_y, p_z) = p$ is the momentum operator, $|kn\sigma\rangle$ the crystal wave function, corresponding to eigen value E_{kn} with crystal momentum k and spin σ. As a final point, f_{kn}, the Fermi distribution function ensures that just transitions from occupied to unoccupied states are counted up, and $\sigma(E_{kn'} - E_{kn} - \omega)$ is the requirement for total energy conservation. The real part $\varepsilon_1(\omega)$ can be gained from the imaginary part $\varepsilon_2(\omega)$ using the Kramer–Kronig's dispersion relation [19]

$$\varepsilon_1(\omega) = 1 + \frac{2}{\pi} P \int_0^{\infty} \frac{\omega' \varepsilon_2(\omega')}{\omega'^2 - \omega^2} d\omega'$$

.

Table 1 Atomic positions

Atoms	$X_{exp.}$	$X_{opt.}$	$Y_{exp.}$	$Y_{opt.}$	$Z_{exp.}$	$Z_{opt.}$
Ag(1)	0.23428 (4)	0.23475	0.31806 (5)	0.3188	0.32726 (3)	0.3276
Ag(2)	0.71991 (6)	0.71940	0.15354 (4)	0.15394	0.57873 (5)	0.57859
Si(1)	0.7199 (3)	0.7190	0.1844 (1)	0.1835	0.0732 (2)	0.0743
Zn(1)	0.22232 (7)	0.22243	0.31373 (7)	0.31384	0.82066 (5)	0.82054
S(1)	0.1161 (1)	0.1139	0.1248 (1)	0.1279	0.5868 (1)	0.5848
S(2)	0.5879 (1)	0.5886	0.3163 (1)	0.3176	0.8534 (1)	0.8501
S(3)	0.0504 (1)	0.0533	0.2008 (1)	0.1989	0.0614 (1)	0.0622
S(4)	0.6239 (1)	0.6232	0.3398 (1)	0.3391	0.2966 (1)	0.2997

3 Results and discussion

3.1 Electronic structure

The self-consistent full-relativistic band structures of the monoclinic phase Ag_2ZnSiS_4 compound are calculated within LDA, GGA, EVGGA and mBJ schemes. The calculated band structures, using the four kinds of exchange correlation, are similar except the values of the band gap which were higher within mBJ. In Fig. 2, we illustrate the electronic band dispersion curves along some high-symmetry directions of the Brillioun zone calculated for the equilibrium geometries of Ag_2ZnSiS_4 compound within LDA, GGA, EVGGA and mBJ approximations. The valence band

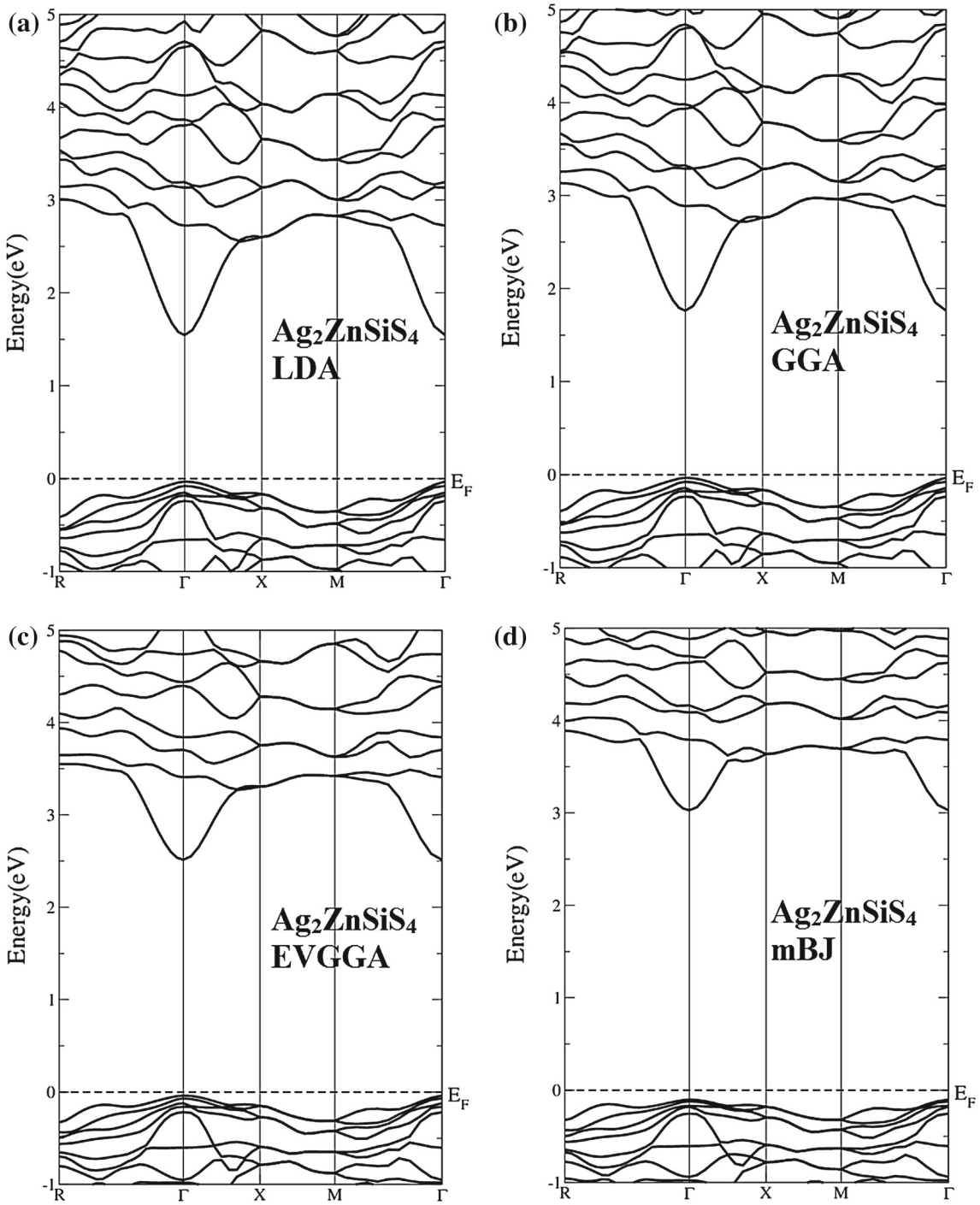

Fig. 2 Calculated band structure

maximum (VBM) and the conduction band minimum (CBM) are positioned at Γ point, resulting in a direct energy band gap. The calculated band gaps are 1.830 (LDA), 2.027 (GGA), 2.715 (EVGGA) and 3.06 (mBJ), respectively. As we have fixed E_F and also the top of VB at $E = 0$ eV, thus, the shifting of bands is expected only in CB in all formalisms. It is observed that the mBJ potential fabricates better band splitting. Thus, the VB and CB shift downwards and upwards, in energy as compared to energy bands in LDA, GGA, EVGGA, such that the difference between CB minimum and VB maximum increases. In this way, the band gaps come closer to corresponding experimental values with mBJ.

We should emphasize that our calculated band gap using mBJ shows better agreement with the experimental value (3.28 eV) [10] than the previous calculation (1.8 eV) [10]. Therefore, we can conclude that mBJ yields an improved band splitting compared to LDA, GGA and EVGGA [20–24]. Thus, for this motive we will discuss the results obtained by mBJ potential only.

Despite considerable efforts in both experimental and theoretical studies [10], it should be pointed out that the previously reported result for the energy gap shows that the calculated energy gap is much less than the measured one. This is attributed to the fact that they have used GGA,

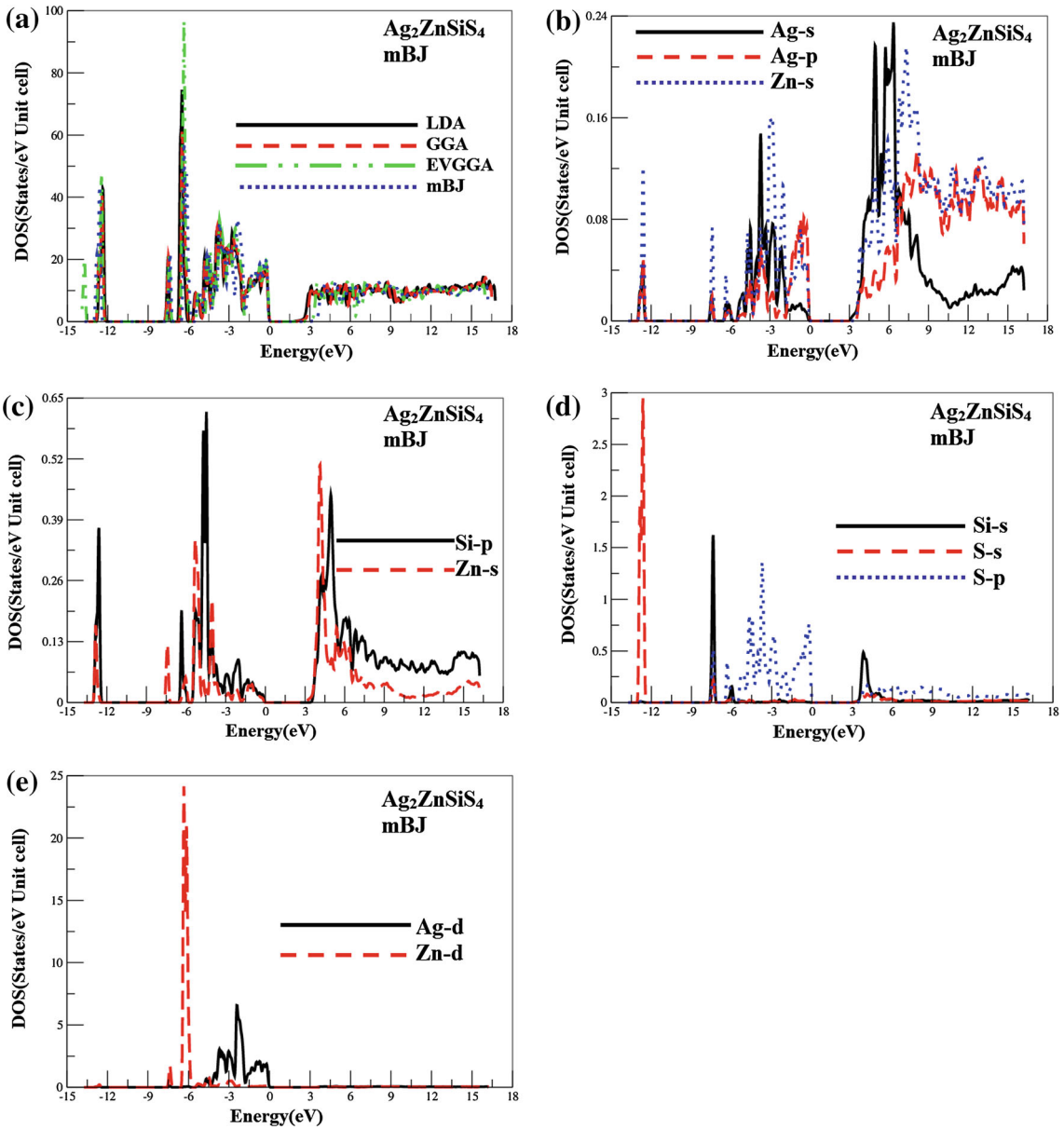

Fig. 3 Calculated total and partial densities of states (states/eV unit cell)

which usually underestimated the band gap. To overcome this drawback, we have used mBJ, which goes beyond GGA. Usually mBJ predicts better lattice constants, bond lengths [25, 26] and phase transitions [27]. Therefore, we have employed mBJ to calculate the band structure, total, partial density of states and optical properties of Ag_2ZnSiS_4 compound.

In order to elucidate the nature of the electronic band structures, we have calculated the total and the partial densities of states (TDOS and PDOS) for this compound which are displayed in Fig. 3. Following Fig. 3, we should highlight that there are three distinct structures separated by gaps. The first structure encountered in the TDOS, starts from −14 to −12 eV consists of S-s with a small contribution of Ag-p, Si-p and Zn-s. The next structure, lying between −8.0 and −0.15 eV is due Si-s, S-p, Zn-d and Ag-d with small contributions from Ag-s/p, Si-p and Zn-s. The third structure from 3.0 and 18.0 eV consist of Si-p and Zn-s with small contributions from Ag-s/p and Zn-s. There exists a strong hybridization between the states; at −13.0 eV there is a strong hybridization between Zn-s and Ag-p states. The Si-s and S-s/p hybridizes at −7.5 eV. At the energy range between −8.0 and −1.0 eV, there is a strong hybridization between Si-p and Zn-s, Ag-s and Zn-s and Ag-s and Ag-p.

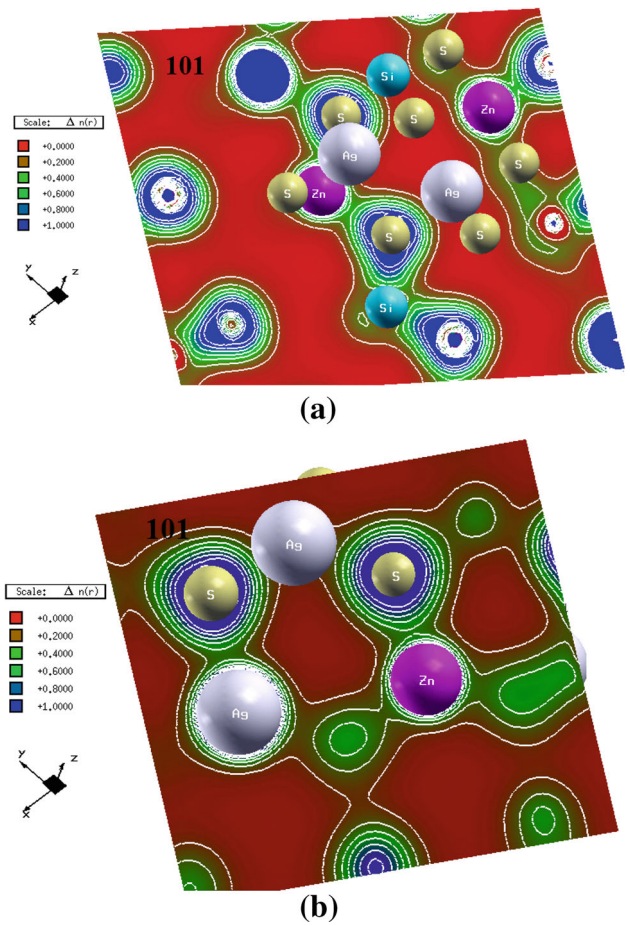

Fig. 4 Electronic charge density contour

3.2 Electronic charge density

In order to comprehend the electronic states of Ag_2ZnSiS_4 compound, the valence electronic charge density plots have been constructed in Fig. 4 along the (101) crystallographic plane. The electron density denotes the nature of the bond [28]. We have predicted the chemical bonding and the charge transfer in Ag_2ZnSiS_4 compound. In Ag_2ZnSiS_4, the bonding has a significant covalent character due to sharing of charge between Zn/Ag and S atoms. It can be perceived that a significant overlapping can be observed between Zn/Ag and S bonding, indicating covalent bonding in Ag_2ZnSiS_4. Moreover, the charge transfer occurs mainly from Zn/Ag atoms towards S atom. The scale shows the concentration of the charge density around the atoms, in which the blue color shows the higher concentration. It is also clear from Fig. 4 that the charge density around S is greater than the other atoms. We have also calculated the bond lengths and the bond angles which show good agreement with the experimental work [10] (see Table 2).

3.3 Optical properties

The optical spectroscopy analysis is a powerful tool to determine of the overall band behavior of a solid [29–31]. In this section of the manuscript, we investigate the optical properties of Ag_2ZnSiS_4 compound, because the study the optical properties of solids has been an interesting research topic in basic research as well as for industrial applications [32]. The optical properties may be obtained from the knowledge of the complex dielectric function $\varepsilon(\omega) = \varepsilon_1(\omega) + i\varepsilon_2(\omega)$. The imaginary part $\varepsilon_2(\omega)$ was calculated from the momentum matrix elements between the occupied and unoccupied wave functions within the assortment rules.

To demonstrate the effect of using different exchange correlation positions on the imaginary (absorptive) and real (dispersive) parts of the dielectric functions, we have calculated the average of the imaginary $\varepsilon_2^{\text{average}}(\omega)$ and the real $\varepsilon_1^{\text{average}}(\omega)$ parts of the dielectric functions using LDA, GGA, EVGGA and mBJ as illustrated in Fig. 5a, b. Following the spectral structure of $\varepsilon_2^{\text{average}}(\omega)$ one can see that the highest spectral peak for the four schemes is situated at energies 4.08, 4.24, 7.90 and 8.47 eV. One can see that all the spectral structure is shifted towards higher energies with higher magnitude, when we move from LDA to GGA, EVGGA then mBJ. We should highlight that since mBJ gives rise to a better band splitting, and hence band gap

Table 2 Bond length

Bond	Distance (A)		Bond	Angle (°)	
	Theor.	Exp.		Theor.	Exp.
Ag(1)–S(1)	2.521	2.537	S(1)–Ag(1)–S(2)	106.82	106.65
Ag(1)–S(2)	2.564	2.5802	S(1)–Ag(1)–S(3)	112.29	112.69
Ag(1)–S(3)	2.522	2.527	S(1)–Ag(1)–S(4)	114.18	114.18
Ag(1)–S(4)	2.503	2.513	S(2)–Ag(1)–S(3)	100.44	100.47
			S(2)–Ag(1)–S(4)	108.69	108.48
			S(3)–Ag(1)–S(4)	113.23	113.14
Ag(2)–S(1)	2.533	2.545	S(1)–Ag(2)–S(2)	110.21	110.08
Ag(2)–S(2)	2.554	2.575	S(1)–Ag(2)–S(3)	110.88	110.86
Ag(2)–S(3)	2.547	2.565	S(1)–Ag(2)–S(4)	106.17	106.46
Ag(2)–S(4)	2.793	2.618	S(2)–Ag(2)–S(3)	106.52	106.14
			S(2)–Ag(2)–S(4)	116.49	117.02
			S(3)–Ag(2)–S(4)	106.54	106.21
Zn(1)–S(1)	2.332	2.327	S(1)–Zn(1)–S(2)	112.06	112.09
Zn(1)–S(2)	2.356	2.354	S(1)–Zn(1)–S(3)	110.67	110.33
Zn(1)–S(3)	2.334	2.333	S(1)–Zn(1)–S(4)	103.94	111.71
Zn(1)–S(4)	2.365	2.3623	S(2)–Zn(1)–S(3)	112.95	112.81
			S(2)–Zn(1)–S(4)	105.28	105.46
			S(3)–Zn(1)–S(4)	103.94	104.08
Si(1)–S(1)	2.150	2.135	S(1)–Si(1)–S(2)	107.50	107.84
Si(1)–S(2)	2.147	2.116	S(1)–Si(1)–S(3)	111.04	111.18
Si(1)–S(3)	2.147	2.122	S(1)–Si(1)–S(4)	109.00	108.5
Si(1)–S(4)	2.152	2.138	S(2)–Si(1)–S(3)	108.98	109.6
			S(2)–Si(1)–S(4)	112.53	111.91
			S(3)–Si(1)–S(4)	107.82	107.8

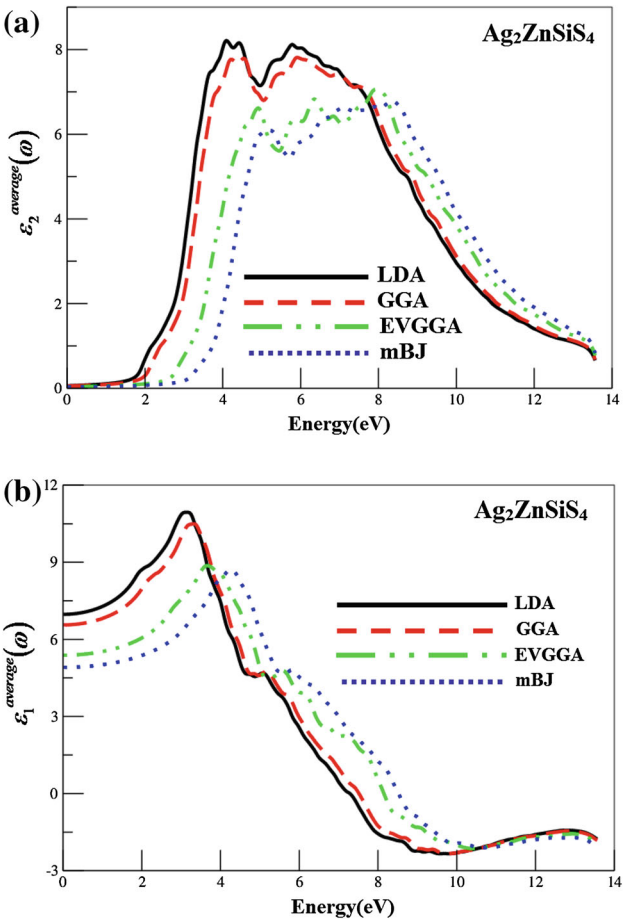

Fig. 5 Calculated imaginary $\varepsilon_2^{\text{average}}(\omega)$and real part $\varepsilon_1^{\text{average}}(\omega)$ of dielectric tensor

closer to the experimental one, this results in better optical transition between the occupied and unoccupied states. Thus, with this objective we will discuss the result of mBJ only. The values of $\varepsilon_1^{\text{average}}(0)$ at the static limit for LDA to GGA, EVGGA then mBJ are 6.92, 6.59, 5.38 and 4.90 eV. These values confirm that the mBJ produce better band gap. We note that a smaller energy gap yields a larger $\varepsilon_1(0)$ value. This could be explained on the basis of the Penn model [33]. Penn proposed a relation between $\varepsilon(0)$ and E_g, $\varepsilon(0) \approx 1 + \left(\hbar\omega_P/E_g\right)^2$. E_g is a kind of averaged energy gap which could be related to the real energy gap. It is clear that $\varepsilon(0)$ is inversely proportional to E_g. Hence, a larger E_g yields a smaller $\varepsilon(0)$.

Since the investigated compound has monoclinic symmetry; therefore, it has five nonzero components of the second-order dielectric tensor. In regardless of this only we will focus on the three major dielectric tensor components $\varepsilon_2^{xx}(\omega)$, $\varepsilon_2^{yy}(\omega)$ and $\varepsilon_2^{zz}(\omega)$ these are the imaginary parts of the frequency-dependent dielectric function. Broadening has been assumed to be 0.1 eV which is normal for the broadening due to the electron–phonon interactions.

The imaginary part of the dielectric function as illustrated in Fig. 6a exhibits different peaks at different photon energies. The origin of these peaks is attributed to the inter-band transitions from the occupied S-s, Si-p, Zn-s/d, and Ag-s/p states to the unoccupied Si-p, Zn-s, and Ag-s/p states. There is isotropy between the three components from 3.0 to 4.5 eV and from 9.5 to 14.0 eV and a considerable anisotropy from 4.5 to 9.5 eV as shown in Fig. 6a. The main peaks in the spectra are located at 5.31, 7.05 and 7.9 eV for $\varepsilon_2^{xx}(\omega)$, $\varepsilon_2^{yy}(\omega)$ and $\varepsilon_2^{zz}(\omega)$, respectively. It is worth noting that for the interpretation of the optical spectra, it does not seem realistic to give a single transition assignment to peaks which are present in these optical spectra since many transitions are found in the band structure with an energy corresponding to the peak.

It is meaningful to make an effort to identify the transitions that are accountable for the intense peak structure in $\varepsilon_2(\omega)$ using our calculated band structure (Fig. 2). The position of the peaks in $\varepsilon_2(\omega)$ together with the foremost contributions from intra-band transitions to each peak disclose the style in which the incident radiation is

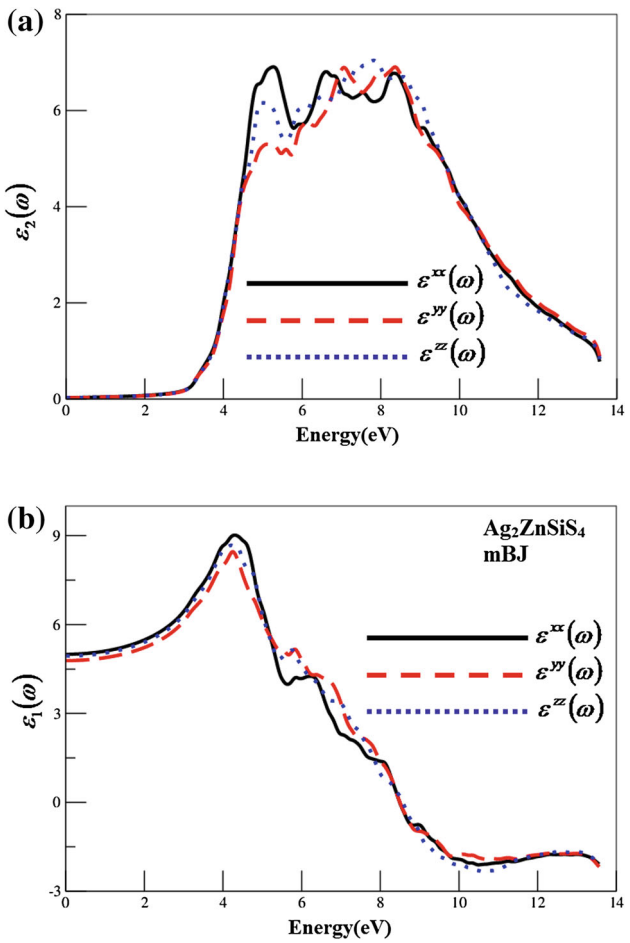

Fig. 6 Calculated imaginary $\varepsilon_2(\omega)$and real part $\varepsilon_1(\omega)$ of dielectric tensor

absorbed in the crystal. The major absorption band is dominated by the transition from S-p states to the s states of Zn and Si atoms as determined from a PDOS analysis, causing considerable energy transfer from sulphur atom to the zinc and silicon atoms.

It would be worthwhile to compare our calculated optical gap (3.06 eV) using mBJ with that (3.28 eV) obtained experimentally using UV/Vis/NIR spectroscopic analysis [10] and good agreement was found. The real part of the dielectric function $\varepsilon_1^{xx}(\omega)$, $\varepsilon_1^{yy}(\omega)$ and $\varepsilon_1^{zz}(\omega)$ which illustrated in Fig. 6b, is obtained from $\varepsilon_2^{xx}(\omega)$, $\varepsilon_2^{yy}(\omega)$ and $\varepsilon_2^{zz}(\omega)$ using the Kramer–Kronig relation. The values of $\varepsilon_1^{xx}(0)$, $\varepsilon_1^{yy}(0)$ and $\varepsilon_1^{zz}(0)$ at the static limit are 4.99, 4.78 and 4.93.

4 Conclusion

In summary, the electronic band structures, electron charge density and optical properties of Ag_2ZnSiS_4 were performed by means of the density functional theory within the LDA, GGA, EVGGA and mBJ. Our calculated atomic positions, energy band gap, chemical bond lengths and angles are in good agreement with experimental data and better the previous calculation. Ag_2ZnSiS_4 presented a direct band gap of 1.830 (LDA), 2.027 (GGA), 2.715 (EVGGA) and 3.06 (mBJ), respectively. The electronic charge density in (101) crystallographic plane was calculated; we found that Zn–S bond possesses a stronger covalent bonding strength than the Ag–S bond. The dielectric optical properties were also calculated and discussed in detail. The relations of the optical properties to the inter-band transitions were also discussed. In the low-energy region, the origins of the spectral peaks are ascribed to the transitions from S-p states to the s states of Zn and Si. We have compared our calculated optical gap (3.06 eV) using mBJ with that (3.28 eV) obtained experimentally using UV/Vis/NIR spectroscopic analysis [10] and good agreement was found.

Acknowledgments The result was developed within the CENTEM project, reg. no. CZ.1.05/2.1.00/03.0088, co-funded by the ERDF as part of the Ministry of Education, Youth and Sports OP RDI programme. School of Material Engineering, Malaysia University of Perlis, Malaysia.

References

1. X. Shi, L. Xi, J. Fan, W. Zhang, L. Chen, Chem. Mater. **22**, 6029–6031 (2010)
2. X.Y. Shi, F.Q. Huang, M.L. Liu, L.D. Chen, Appl. Phys. Lett. **94**, 122103 (2009)
3. C. Steinhagen, M.G. Panthani, V. Akhavan, B. Goodfellow, B. Koo, B.A. Korgel, J. Am. Chem. Soc. **131**, 12554–12555 (2009)
4. J.W. Lekse, M.A. Moreau, K.L. McNerny, J. Yeon, P.S. Halasyamani, J.A. Aitken, Inorg. Chem. **48**, 7516–7518 (2009)
5. W. Ruderman, J. Maffetone, D. Zelman, D. Poirier, Mater. Res. Soc. Symp. Proc. **484**, 519–524 (1998)
6. G. Catella, D. Burlage, MRS Bull. **23**, 28–36 (1998)
7. E. Parthe, *Crystal chemistry of tetrahedral structures* (Gordon and Breach Science Publishers, New York, 1964)
8. N.A. Goryunova, in ed. by J.C. Anderson, The Chemistry of Diamond-like Semiconductors, (The M.I.T. Press, Cambridge, 1965) (Chapters 1–3)
9. L. Pauling, J. Am. Chem. Soc. **51**, 1010–1026 (1929)
10. C.D. Brunetta, B. Karuppannan, K.A. Rosmus, J.A. Aitken, J. Alloy. Compd. **516**, 65–72 (2012)
11. P. Blaha, K. Schwarz, J. Luitz WIEN97, A full potential linearized augmented plane wave package for calculating crystal properties, Karlheinz Schwarz, Techn. Universit at Wien, Austria, ISBN:3-9501031-0-4 (1999)
12. P. Hohenberg, W. Kohn, Phys. Rev. **136**, B864 (1964)
13. W. Kohn, L.J. Shom, Phys. Rev. **140**, A1133 (1965)
14. J.P. Perdew, A. Zunger, Phys. Rev. B. **23**, 5048 (1981)
15. J.P. Perdew, K. Burke, M. Ernzerhof, Phys. Rev. Lett. **77**, 3865 (1996)
16. E. Engel, S.H. Vosko, Phys. Rev. **B50**, 10498 (1994)
17. A.D. Becke, E.R. Johnson, J. Chem. Phys. **124**, 221101 (2006)
18. A. Delin, P. Ravindran, O. Eriksson, J.M. Wills, Int. J. Quant. Chem. **69**, 349 (1998)

19. W.T. Ching, P. Rulis, Phys. Rev. **B73**, 045202 (2006)
20. A.H. Reshak, H. Kamarudin, I.V. Kityk, S. Auluck, J. Mater. Sci. **48**, 5157–5162 (2013)
21. S. Azam, A.H. Reshak, Int. J. Electrochem. Sci. **8**, 10359–10375 (2013)
22. A.H. Reshak, S.A. Khan, Comput. Mater. Sci. **78**, 91–97 (2013)
23. S.A. Khan, A.H. Reshak, Int. J. Electrochem. Sci. **8**, 9459–9473 (2013)
24. W. Khan, A. H. Reshak J. Mater. Sci. doi: 10.1007/s10853-013-7798-3
25. J.P. Perdew, Y. Wang, Phys. Rev. B **45**, 13244 (1992)
26. R. Asahi, Y. Taga, W. Mannstadt, A.J. Freeman, Phys. Rev. B **61**, 7459 (2000)
27. M.D. Segall, P.J.D. Lindan, M.J. Probert, C.J. Pickard, P.J. Hasnip, S.J. Clark, M.C. Payne, J. Phys. Condens. Matter **14**, 2717 (2002)
28. S. Azam, A.H. Reshak, Phys. B **431**, 102–108 (2013)
29. B. Amin, R. Khenata, A. Bouhemadou, I. Ahmad, M. Maqbool, Phys. B **407**, 2588–2592 (2012)
30. B. Amin, I. Ahmad, M. Maqbool, S. Goumri-Said, R. Ahmad, J. Appl. Phys. **109**, 023109 (2011)
31. M. Maqbool, B. Amin, I. Ahmad, J. Opt. Soc. Am. B **26**(11), 2181–2184 (2009)
32. A.H. Reshak, S. Azam, Int. J. Electrochem. Sci. **8**, 10396–10423 (2013)
33. D.R. Penn, Phys. Rev. B. **128**, 2093 (1962)